Biosensors and Bioelectronics 141 (2019) 111386

Contents lists available at ScienceDirect

Biosensors and Bioelectronics

journal homepage: www.elsevier.com/locate/bios

Direct monitoring of breast and endometrial cancer cell epigenetic response to DNA methyltransferase and histone deacetylase inhibitors

S.R. Teixeira[b,c], C.M. Abreu[d], L. Parkes[a,c], J. Davies[a,c], S. Yao[a,c], M.A. Sawhney[a,c], L. Margarit[a,e], D. Gonzalez[a,c], I. Mendes Pinto[d], L.W. Francis[a,c], R.S. Conlan[a,c,*]

[a] Swansea University Medical School, Singleton Park, Swansea, SA2 8PP, UK
[b] College of Engineering, Swansea University, Bay Campus, Swansea, SA1 8QQ, UK
[c] Centre for NanoHealth, Swansea University, Singleton Park, Swansea, SA2 8PP, UK
[d] International Iberian Nanotechnology Laboratory (INL), Portugal
[e] Abertawe Bro Morganwg University Health Board, Princess of Wales Hospital Bridgend, UK

ARTICLE INFO

Keywords:
Epigenetics
EIS
DNA methylation
Histone acetylation
Cancer cell lines

ABSTRACT

DNA methylation and histone deacetylation are key epigenetic processes involved in normal cellular function and tumorigenesis. Therapeutic strategies based on DNA methyltransferase (DNMT) and histone deacetylase (HDAC) inhibitors are currently in use and under development for the treatment of cancers. Genome-wide DNA methylation profiling has been proposed for use in disease diagnosis, and histone modification profiling for disease stratification will follow suit. However, whether epigenome sequencing technologies will be feasible for rapid clinic diagnosis and patient treatment monitoring remains to be seen, and alternative detection technologies will almost certainly be needed. Here we used electrochemical impedance spectroscopy (EIS) employing a graphene-based screen-printed electrode system to directly measure global DNA methylation and histone H3 acetylation to compare non-cancer and breast cancer cell lines. We demonstrated that whilst global methylation was not useful as a differential marker in the cellular systems tested, histone H3 acetylation was effective at higher chromatin levels. Using breast and endometrial cancer cell models, EIS was then used to monitor cellular responses to the DNMT and HDAC inhibitors 5-Aza-2′-deoxycytidine and suberoylanilide hydroxamic acid *in vitro*, and proved very effective at detecting global cellular responses to either treatment, indicating that this approach could be useful in following treatment response to epigenetic drugs. Moreover, this work reports the first combined analysis of two epigenetic markers using a unified graphene-based biosensor platform, demonstrating the potential for multiplex analysis of both methylation and acetylation on the same sample.

1. Introduction

Cancer cells undergo epigenetic changes in 5-methylcytosine distribution that include global DNA hypomethylation and the hypermethylation of promoter CpG islands associated with tumor-suppressor genes. DNA methylation is just one facet in the coordinated regulation of chromatin structure that also involves discrete modifications to histone proteins, including histone H3 and H4 deacetylation, among others, which collectively result in transcriptionally altered states (Capp, 2017; Jones and Baylin, 2007; Lo and Zhou, 2018; Sheahan and Ellis, 2018).

Large-scale epigenomic studies have been made possible using established complex technologies. These allow the genome-wide mapping of epigenetic marks, including DNA methylation and histone modifications, which are critical for regulating gene expression. In turn, we are learning how mapping aberrant alterations to these epigenetic marks can be used in clinical diagnostics (Bock et al., 2016; Butler and Dent, 2013; Libertini et al., 2016; Rendeiro et al., 2016).

DNA methylation and histone modification biomarkers have several advantages that qualify them for broad use as *in vitro* diagnostics and to support clinical decisions: (i) They can be cell-type-specific, yet robust toward transient perturbations. (ii) They are binary marks (i.e., for a single cell and allele, an epigenetic mark is either modified or not), which facilitates reliable measurements on heterogeneous samples. (iv) The use of epigenetic markers to detect cancer sensitively is based on the premise that tumor-derived chromatin/DNA is released into bodily fluids, or other remote samples, and can be detected by abnormal DNA methylation and histone modification patterns (Bormann et al., 2018;

* Corresponding author. Swansea University Medical School, Singleton Park, Swansea, SA2 8PP, UK.
E-mail address: r.s.conlan@swansea.ac.uk (R.S. Conlan).

https://doi.org/10.1016/j.bios.2019.111386
Received 11 April 2019; Received in revised form 23 May 2019; Accepted 30 May 2019
Available online 12 June 2019
0956-5663/

Coleman and De, 2018; Graff-Baker et al., 2018; Singh et al., 2018; Xi et al., 2018; Zhang et al., 2018).

Current approaches to assess the epigenetic state currently target individual genetic loci to determine histone modification (predominantly acetylation and methylation) and DNA methylation status. Bisulphite sequencing has been the mainstay of DNA methylation analysis with methylated and hydroxymethylated DNA immunoprecipitation (MeDIP and (h)MeDIP) methods coming online, whilst chromatin immunoprecipitation (ChIP) is the research tool of choice for determining histone modifications. However, these approaches are yet to become a clinically useful diagnostic methods due to their time-consuming nature, and where genome-wide DNA sequencing is used (bisulphite and ChIP/MeDIP – seq), the generation of more data than is needed for diagnosis or monitoring therapeutic response. Other approaches include serum proteomics using mass spectrometry that whilst progressing in clinical feasibility studies, require expensive and highly technical hardware, and expert users for sample and data analysis.

Electrochemical immunosensors using advances in nanomaterials are being developed for biosensing applications (Zhu et al., 2015). For the detection of epigenetic modifications electrochemical analytical methods offer several advantages over other techniques, such as surface plasmon resonance and atomic force spectroscopy, in terms of sensitivity, simplicity and portability (Stewart and Tsui, 2018). Furthermore, they offer limits of detection of methylated DNA within the levels reported to be found circulating in plasma (Stewart and Tsui, 2018). In addition, instrumentation required to make such measurements is low-cost, with instrument refinement reducing costs even further (Sawhney and Conlan, 2019). Gold and carbon -based electrode systems remain the most utilized working electrode materials, despite many other materials having been evaluated (Krejcova et al., 2017), and have been used in screen printed formats that offer low cost per unit, and do not require extensive preparation to obtain a pristine surface prior to use. Graphene as a working electrode offers a high signal to noise ratio, and is easily functionalized with antibodies when coated with polyaniline, which also serves a conductive polymer and is used as an additive transducer layer to avoid the introduction of graphene surface defects (Gazze et al., 2018; Teixeira et al., 2014a). Graphene offers a further advantage over gold electrodes for the detection and quantification of DNA as it lacks the inherent absorption properties for unmodified DNA that are displayed by gold surfaces due to affinity interactions (Koo et al., 2015). Here, we demonstrate the use of a graphene-based immunosensor, where anti-5-methylcytosine (anti-5mc) and anti-acetylated histone H3 (anti-acH3) antibodies were directly coupled to a polyaniline-modified screen-printed graphene electrode to detect DNA and chromatin using label-free EIS measurements. Using this system global levels of methylated DNA and histone H3 acetylated chromatin levels were assessed in non-cancer (MCF12A) and cancer (MCF7) breast cell models, and MCF7 and HEC50 endometrial cancer cells treated with a DMNT or HDAC inhibitors were found to show alterations in DNA methylation or histone H3 acetylation respectively. Overall, this study highlights the effectiveness EIS graphene immune sensors for the direct label- and amplification-free detection of global epigenetic modifications in cancer cells, and thus their potential for monitoring therapeutic efficacy.

2. Materials and methods

Cell culture and treatments. MCF7 cells (ATCC, Maryland, USA) were cultured in Eagle's Minimum Essential Medium (Gibco, ThermoFisher Scientific, UK) supplemented with 10% (v/v) foetal bovine serum (Gibco) and 0.01 mg/ml insulin (Sigma-Aldrich, Missouri, USA). Hec50 cells (ATCC) were cultured in Dulbecco's Modified Eagle Medium: Nutrient Mixture F-12 (DMEM/F12) (Gibco) supplemented with 10% (v/v) fetal bovine serum (Gibco), 1% (v/v) penicillin and streptomycin (Gibco), sodium bicarbonate and sodium pyruvate. MCF12A cells (ATCC) were cultured in Dulbecco's Modified Eagle Medium: Nutrient Mixture F-12 (DMEM/F12) (Gibco) supplemented with 5% (v/v) horse serum (Gibco), 20 ng/ml human epidermal growth factor, 100 ng/ml cholera toxin, 0.01 mg/ml bovine insulin and 500 ng/ml hydrocortisone 95%. All cell lines were grown at 37 °C in a humidified atmosphere with 5% CO2 to 90% confluency in T75 flasks (Corning, New York, USA) before collection. Cells were grown to 40% or 60% confluency respectively before exchanging full growth media for stripped media prior to treatment with the DNMT inhibitor 5-Aza-2′-deoxycytidine (1 μM), suberoylanilide hydroxamic acid (2.5 μM) or vehicle (DMSO).

Chromatin and genomic DNA extraction. Chromatin and gDNA were extracted using the Chromatrap® ChIP seq kit chromatin preparation reagents and the Chromatrap® MeDIP kit gDNA preparation reagents according to the manufacturer's instructions (Porvair Sciences Ltd, Wrexham, UK).

Immunosensor assembly. Graphene-SPEs were purchased from DropSens (DRP-110GPH, Metrohm, UK Ltd, Runcorn, UK) and were composed of a carbon counter electrode, a silver pseudo-reference electrode, and a printed graphene working electrode (4 mm ∅). Electrical characterization of SPEs was performed by connecting the SPEs to the potentiostat/galvanostat *via* a suitable switch box (DropSens). In order to mediate selective immunodetection of chromatin and gDNA to the graphene sensor surface, PANI functionalization was utilized, as previously described (Teixeira et al., 2014b).

Electrochemical measurements. CV and EIS were performed using a Metrohm Autolab PGSTAT302N equipped with FRA32M and DRP-DSC connector; control and analysis were provided through Nova software version 2.0.1 and higher (Metrohm). CV procedures spanned −0.7 to 0.7 V starting and ending at 0V with a scan rate of 0.05 V per second. EIS procedures applied 50 frequencies between 1000 and 0.01 Hz, logarithmically distributed at an amplitude of 0.01 V_{RMS} on a DC bias of 0.1V with the reference electrode. EIS data was fitted to a R(C[R(RC)]) equivalent circuit model using a maximum of 300 iterations with weight factor applied.

Chromatin/gDNA detection and quantification. The functionalized biosensing platforms are based on impedance measurements resulting in changes of resistivity (Rct) following the binding of a chromatin or gDNA to the specific antibody immobilized on the sensor surface. Increasing concentrations of chromatin ranging from 0.0086 to 134 ng/μL for MCF12A, 0.0078–123 ng/μL for MCF7 and 0.0053–416 ng/μL for Hec50; and gDNA solutions, ranging from 0.0048 to 75 ng/μl for all cell lines, were prepared by dilution of 1708 ng/μL of chromatin and 75 ng/μL of gDNA stock solutions in media.

Chromatin immunoprecipitation. ChIP assays were performed using the Chromatrap® ChIP-seq kit following the manufacturers' instructions (Porvair Sciences). Chromatin was quantified by Nanodrop 2000 (ThermoFisher Scientific, UK) and visualized using by agarose gel electrophoresis to ensure correct distribution of fragment sizes prior to immunoprecipitation. 1 μg of each chromatin sample was used per ChIP with 2 μg of relevant antibody; anti acetyl H3 antibody (Millipore, Darmstadt, Germany) or non-specific rabbit IgG (Porvair Sciences). qPCR was carried on the target gene *p21 forward primer* 5′-CCCACAG CAGAGGAGAAAGAA; *reverse primer* 5′-CTGGAAATCTCTGCCAGACA.

Methylated DNA immunoprecipitation. MeDIP assays were carried out using the Chromatrap MeDIP kit according to the manufacturers' protocol (Porvair Sciences). gDNA was quantified by Nanodrop 2000 (ThermoFisher Scientific) and visualized using agarose gel electrophoresis to ensure correct distribution of fragment sizes prior to immunoprecipitation. 500 ng DNA was used per MeDIP with 1 μg kit supplied anti-5-methylcytosine antibody or non-specific mouse IgG and linker. Samples were neutralized, and amplification of enriched methylated DNA carried out at the *CXCL12* locus *forward primer* 5′-CTCA TTCAGTTCCCGCCATC; *reverse primer* 5′-GCCGCTTATTGTCCCTGTG.

Protein blotting. Total protein was extracted using RIPA buffer and quantified using the DC Protein assay (BioRad, Watford, UK). Relevant

protein concentrations were separated by SDS PAGE. Proteins were transferred to PVDF membrane, blocked and probed with a 1/15,000 dilution of anti-acetyl H3 antibody (Millipore, Watford, UK) followed by ECL anti-rabbit IgG horse radish peroxidase (GE Healthcare, Bucks, UK). Bands were developed using the Clarity Western ECL Substrate (Biorad) chemiluminescence kit and visualized using a ChemiDoc (BioRad).

Dot blotting. gDNA extracted and sheared as described for the MeDIP protocol was used for dot blotting. Immun-Blot PVDF Membrane (BioRad) was activated with methanol and equilibrated with transfer buffer prior to spotting the membrane with 100 ng heat denatured gDNA. A 1/300 dilution of the primary antibody anti-5mC (Porvair Sciences) was used to probe the methylated DNA and detected with ECL anti-rabbit IgG horse radish peroxidase (GE Healthcare).

3. Results

3.1. Immunosensor assembly and functionalization

Electrochemical impedance spectroscopy (EIS) is a label and amplification free technique that enables direct molecular measurements on modified surface electrodes (Sánchez et al., 2008). Here, we adapted our previously reported screen-printed electrode (SPE)-graphene/polyaniline (PANI) platform to detect methylated DNA and acetylated histone H3 using anti-5mc and anti-acH3 antibodies respectively. Sensor optimization using control DNA and chromatin extracted from cell line models established sensitivity according to our established protocols (Teixeira et al., 2016).

Sensor assembly was evaluated using scanning electron microscopy and atomic force microscopy (Fig. S1), and electron transfer properties determined against a redox probe and evaluated by cyclic voltammetry (CV) and EIS. Unmodified graphene-SPEs showed a quasi-reversible electrochemical response for the $[Fe(CN)_6]^{3-/4-}$ redox couple with ΔEp of 0.158 V and ΔIp of 0.285 mA, respectively. After 10 cycles, the modification of graphene-SPE surface with PANI resulted in a ΔIp increase of 0.894 mA and a ΔEp decrease of 2.898 V (Fig. 1A) attributed to positively charged amino groups of the PANI molecule attracting the negative charge of $[Fe(CN)_6]^{3-/4-}$ promoting electron transfer on the electrode surface (Zor et al., 2013). A cyclic voltammogram of the SPE-graphene/PANI/Antibody electrode showed a decrease peak-to-peak potential separation (ΔEp of 0.547 V). Further, addition of the BSA blocking agent to the SPE-graphene/PANI/Ab electrode surface gave rise to a change on the electrochemical behavior of $[Fe(CN)_6]^{3-/4-}$, leading to a ΔEp increase of 0.258 V and decreased ΔIp value of 0.546 mA. BSA molecules cause masking of the electrode surface oxidation/reduction of the redox probe $[Fe(CN)_6]^{3-/4-}$ (Daniels and Pourmand, 2007).

EIS data are presented as Nyquist plots where the Rct at the electrode surface is given by the hemicircle diameter obtained in EIS and can be used to define the interface properties of the electrode. The unmodified graphene surface display fast electron-transfer properties (Rct = 884 Ω, Fig. 1B), which increases following PANI deposition (Rct = 1.13 KΩ, Fig. 1B). Following covalent attachment of anti-acH3 antibody, the Rct increased to 1.82 KΩ (Fig. 1B), demonstrating that electron exchange between the redox probe and the electrode was impeded, and this was enhanced further when BSA was added to the SPE-graphene/PANI/Ab (Rct = 2.09 KΩ, Fig. 1B). Similar data was obtained for the anti-5mc antibody sensor platform build (Fig. 1C and D). To define linear ranges for 5mc and acH3 concentrations, Rct values of genomic DNA (gDNA; 4.8pg/μL - 75ng/μL) and chromatin (8.6pg/μL - 134ng/μL) were determined (Fig. 2A and B respectively).

3.2. DNA methylation and histone H3 acetylation status in normal and breast cancer cell models

Global and locus specific epigenetic profiles were determined for non-cancer (MCF12A) and cancer derived (MCF7) breast cell lines. EIS demonstrated resistance due to presence of methylated DNA present in chromatin extracts from MCF7 (e.g., 2630 Ω ± 160 Ω; 75 ng/μL input gDNA) and MCF12A cells (2510 Ω ± 205 Ω; 75 ng/μL input gDNA) (Fig. 3A), consistent with global methylated DNA assessment made using dot blotting (Fig. 3B). Single locus analysis of a CpG island in the 5′UTR of CXCL12, which encodes the stromal cell derived factor 1α protein commonly overexpressed in many cancers (Guo et al., 2016), also demonstrated that DNA methylation levels were similar in both normal and cancer breast cell types (Fig. 3C).

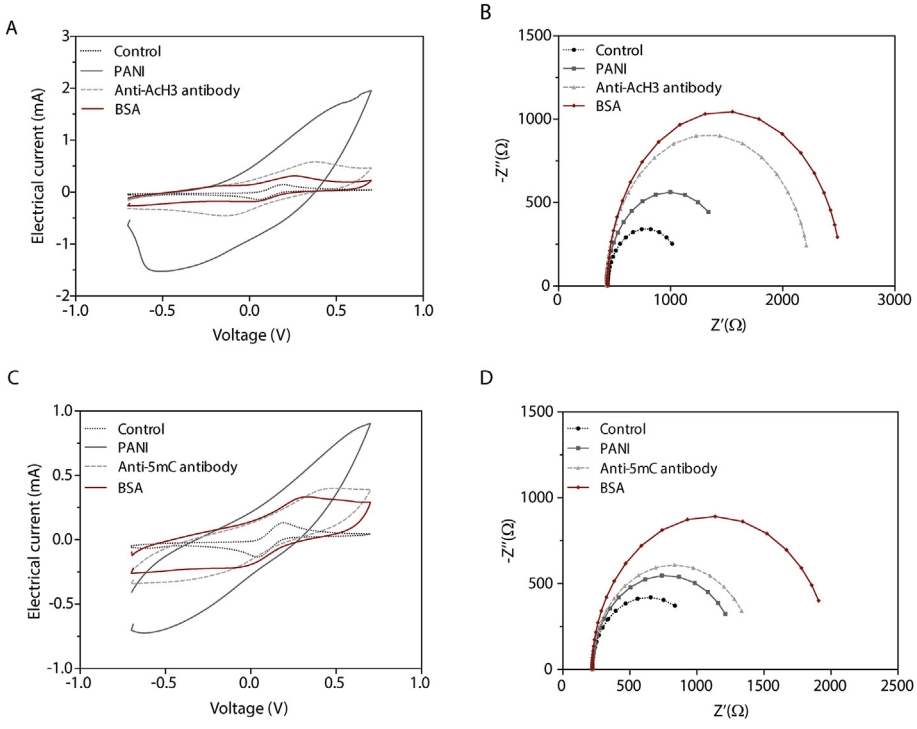

Fig 1. Electrochemical characterization of biosensor assembly. (A) Cyclic voltammogram (CV) of the acetylation immunosensor assembly after each modification of graphene-SPE/PANI//anti-acH3/BSA. (**B**) Nyquist plots of graphene-SPE/PANI//anti-acH3/BSA sensor obtained in 5.0 mM $[Fe(CN)_6]^{3-/4-}$ PBS buffer pH 7.4. (**C**) CV of the methylation immunosensor assembly after each modification of graphene-SPE/PANI//anti-5mC/BSA (**D**) Nyquist plots of graphene-SPE/PANI/anti-5mC/BSA sensor, obtained in 5.0 mM $[Fe(CN)_6]^{3-/4-}$ PBS buffer pH 7.4.

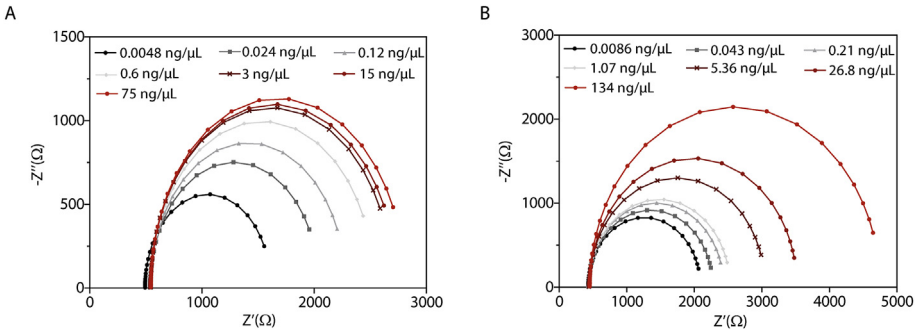

Fig. 2. Global epigenetic modifications in breast cells (MCF12A). (**A**) Representative Nyquist plot of the methylation biosensor upon detection of increasing concentrations of gDNA (**B**) Representative Nyquist plot of the acetylation biosensor upon detection of increasing concentrations of chromatin.

EIS also enabled direct measurement of global histone H3 acetylation (acH3) in MCF7 cells for e.g., 4460 Ω ± 50 Ω, 134 ng/µL input chromatin which was significantly higher than the levels measured in MCF12A (3287 Ω ± 589 Ω, 75 ng/µL input chromatin) (Fig. 3D), and this difference was confirmed by protein blotting (Fig. 3E). Conversely ChIP analysis at the cyclin dependent kinase inhibitor 1 (p21) locus revealed an 8-fold lower level in acetylation in MCF7 compared to MCF12A cells (Fig. 3F), demonstrating that whilst globally the MCF7 genome is hyperacetylated compared to MCF12A cells, there are also locus specific and therefore functional differences between these breast cell lines. Suppression of p21 expression through loss of acetylation results in loss of cell cycle arrest, driving proliferation, a hallmark of cancer cells, and is therefore expected in the cancer cell line.

EIS sensor measurements show that global measurement of epigenetic marks can be useful in differentiating cancer and non-cancer cell types, and that combining epigenetic signatures may be beneficial. For example, MCF7 (low methylation + high acetylation) can be distinguished from MCF12A (low methylation + low acetylation). With the addition of other epigenetic marks an algorithm could be developed to provide a cell specific signature.

3.3. Monitoring global response to decitabine and vorinostat treatments in cancer cell lines

Small chemical modifications that trigger chromatin remodeling through processes including DNA methylation and histone acetylation

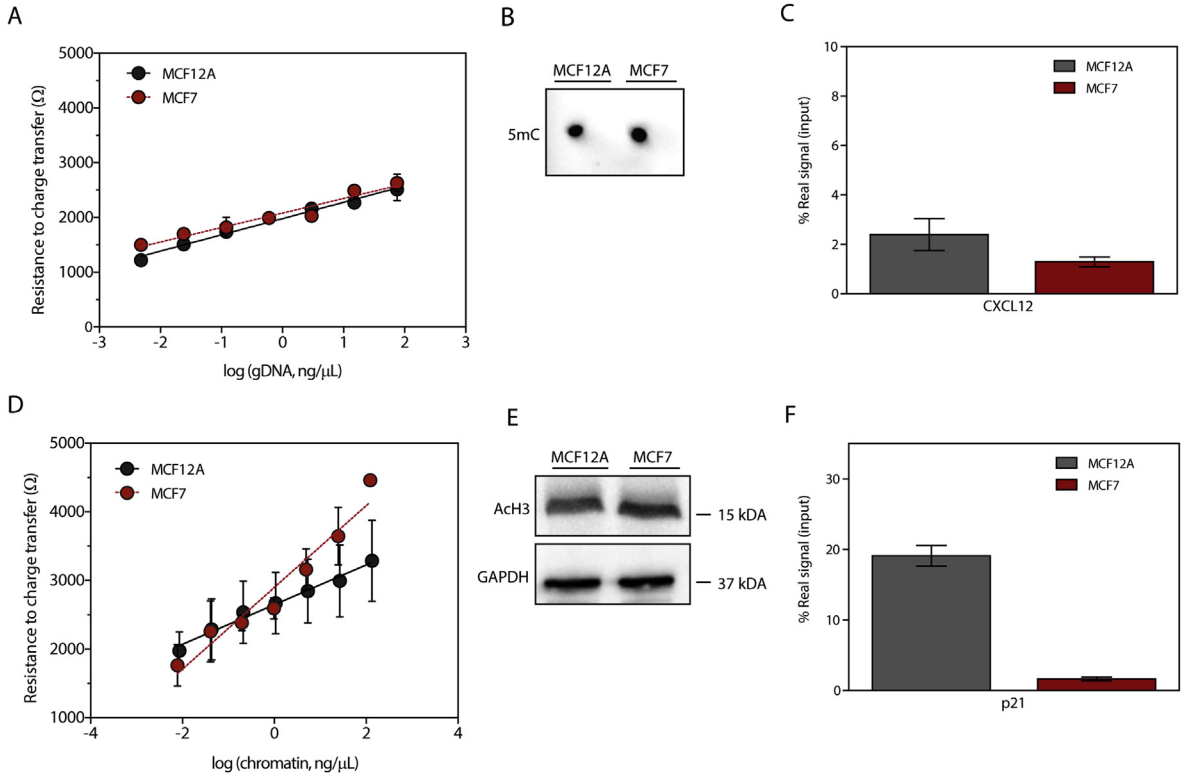

Fig. 3. Detection of global (A, B, D and E) and locus (C and F) modifications in breast cancer cells. (**A**) Calibration curve, plotting log(gDNA) against Rct for MCF12A and MCF7. Error bars represent the standard error of the mean of three biological replicates. (**B**) Dot blotting of global methylation for MCF12A versus MCF7 using gDNA with anti-5mC antibody. (**C**) MeDIP enrichment of CXCL12 from 500 ng MCF12A and MCF7 gDNA by MeDIP using anti-5mC antibody relative to a non-specific IgG reported as % real signal (% positive antibody - % IgG, relative to a standard gDNA input sample). Error bars represent the standard error of the mean of three biological replicates. (**D**) Calibration curve, plotting log(chromatin) against Rct for MCF12A and MCF7. Error bars represent the standard error of the mean of three biological replicates. (**E**) Protein blot detection of global acetylated histone H3 (acH3) in MCF12A and MCF7 chromatin using a specific antibody directed against the modified histone protein. (**F**) Enrichment of the human p21 locus associated with acetylated histone H3 by ChIP using 1 µg MCF12A and MCF7 chromatin. Error bars represent the standard error of the mean of three biological replicates.

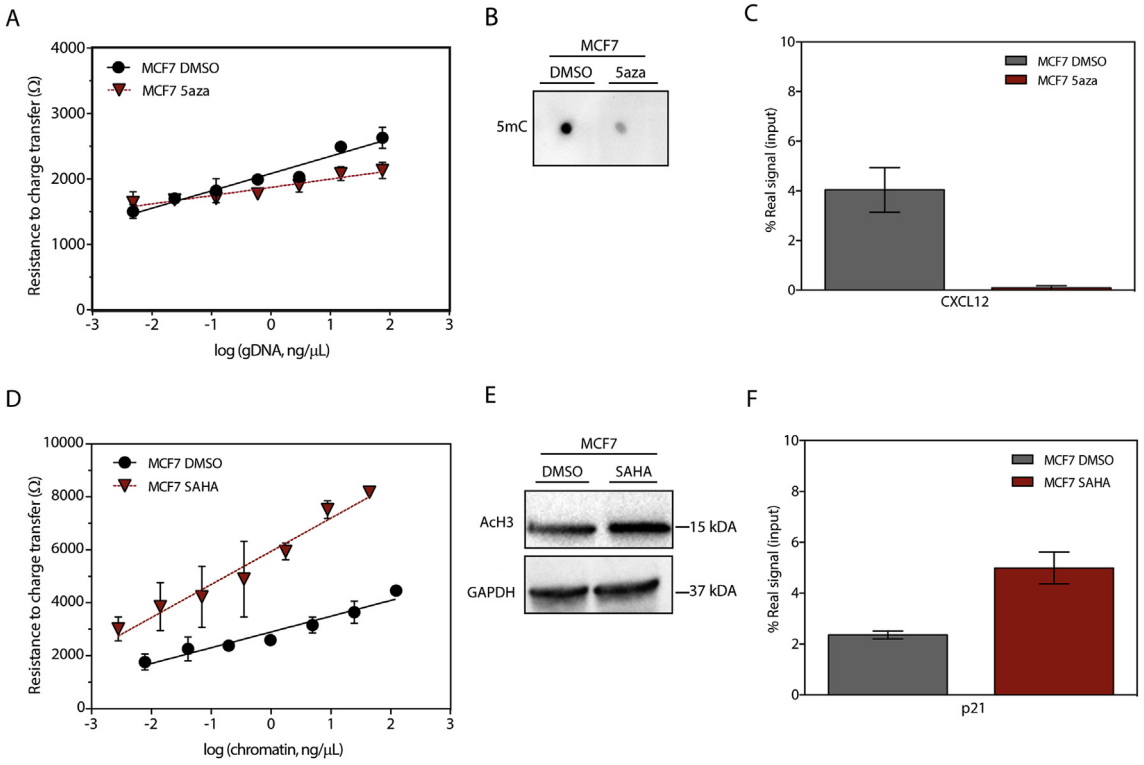

Fig. 4. Detection of global (A, B, D and E) and locus (C and F) modifications in breast cancer cells (MCF7) upon treatment. (**A**) Calibration curve, plotting log (gDNA) against Rct for MCF7 treated versus MCF7 untreated. Error bars represent the standard error of the mean of three biological replicates. (**B**) Dot blotting of global methylation for MCF7 treated versus untreated using gDNA with anti-5mC antibody. (**C**) MeDIP enrichment of CXCL12 from 500 ng MCF7 treated and MCF7 untreated gDNA using anti-5mC antibody relative to a non-specific IgG. Error bars represent the standard error of the mean of three biological replicates. (**D**) Calibration curve, plotting log(chromatin) against Rct for MCF7 treated versus MCF7 untreated. Error bars represent the standard error of the mean of three biological replicates. (**E**) Protein blot detection of global acetylated histone 3 (acH3) in MCF7 treated versus untreated chromatin using a specific antibody directed against the modified histone protein. (**F**) Enrichment of the human p21 locus associated with acetylated histone H3 by ChIP using 1 μg MCF7 treated and MCF7 untreated chromatin. Error bars represent the standard error of the mean of three biological replicates.

are of increasing interest as therapeutic targets in cancer diseases due to reversible nature of these epigenetic modifications (Dawson and Kouzarides, 2012; Flavahan et al., 2017). For example, 5-Aza-2′-deoxycytidine (decitabine) is a strong inducer of DNA de-methylation and is approved for the treatment of myelodysplastic syndrome (Mossman et al., 2010; Ramos et al., 2015), and suberoylanilide hydroxamic acid (vorinostat) is a histone deacetylase inhibitor (HDACi) approved for the treatment of cutaneous T cell lymphoma (Qu et al., 2017). The rapid detection of global epigenetic status could represent a useful tool for risk assessment, diagnosis, and for treatment monitoring, complementing locus specific analysis of tumor suppressor and oncogene epigenetic status in patients.

EIS was used to assess MCF7 and HEC50 cells for response to decitabine and vorinostat treatments (Fig. 4A and D; Fig. 5A and D). The response of MCF7 cells to decitabine was readily distinguished using EIS sensors at higher concentrations of input gDNA (≥ 15ng/μL). For example, a ΔΩ between untreated (2630 Ω ± 160 Ω at 75 ng/μL) compared to treated (2130Ω ± 122 Ω at 75ng/μL) was −500Ω showing an expected decrease in DNA following treatment. For endometrial cancer cells (HEC50) a similar trend was observed, for example a mean ΔΩ of −780 at 75ng/μL (Fig. 5A).

These responses were validated using a methylated DNA specific dot blot, where 100 ng total gDNA extracted from both MCF7 and HEC50 cells showed decreased intensity following treatment (Figs. 4B and 5B), and by MeDIP where the CpG island region of the CXCL12 gene was significantly demethylated. A 45-fold decrease in DNA methylation was measured by MeDIP in MCF7 cells, whereas in HEC50 only a 3-fold decrease in methylation was observed (Figs. 4C and 5C).

Acetylated histone H3 was similarly analyzed following exposure of cells to vorinostat. Significantly increased acetylation was observed in the treated samples compared to untreated controls in both MCF7 and HEC50 with ΔΩ much greater compared to that observed for decitabine treatment (Figs. 4D and 5D). For MCF7, a ΔΩ of +653 (8173 Ω ± 99 Ω treated, 7520 Ω ± 331 Ω untreated) was measured at the highest input chromatin concentration of 24.6 ng/μL for untreated and 44 ng/μL for vorinostat treated cells, indicative of an increase in open chromatin architecture. For HEC50, a ΔΩ of +4600 (7830 Ω ± 90 Ω treated, 3230Ω ± 38 Ω untreated) was obtained for 83.2 ng/μL for untreated cells and 58 ng/μL for treated cells.

Immunosensor performance was also validated by protein blotting (Figs. 4E and 5E), and p21 ChIP where a 2.11 and 3.28 -fold increase in H3 acetylation following vorinostat treatment were measured in MCF7 and HEC50 respectively (Figs. 4F and 5F).

The use of EIS in monitoring cellular responses to drug treatment is clearly very effective, and such a monitoring would be of value in determining patient responses to such treatments, particularly if measurements could be made directly from free circulating methylated DNA and modified chromatin that are known to alter in patients.

4. Discussion

The adaptation of a graphene based EIS immunosensor has enabled for the first-time direct amplification-free and label-free detection of both DNA- and nucleosome-linked epigenetic modifications. The method developed here utilizes antibodies that have been validated and widely used for locus specific genome wide analysis associated with ChIP- and MeDIP- techniques, making comparison between EIS and epigenomic analysis more robust. The EIS method presents a snapshot

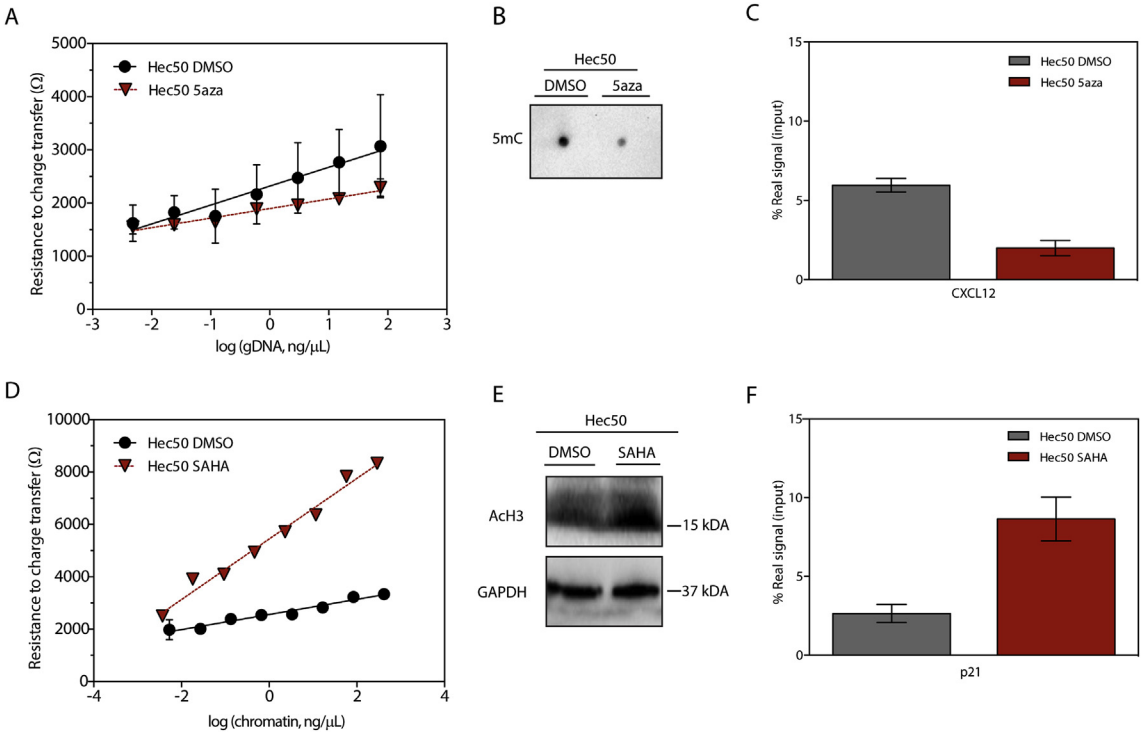

Fig. 5. Detection of global (A, B, D and E) and locus (C and F) modifications in endometrial cells (HEC50) upon treatment. (**A**) Calibration curve, plotting log (gDNA) against Rct for HEC50 treated versus Hec50 untreated. Error bars represent the standard error of the mean of three biological replicates. (**B**) Dot blotting of global methylation for HEC50 treated versus HEC50 untreated using gDNA with anti-5mC antibody. (**C**) MeDIP enrichment of CXCL12 from 500 ng HEC50 treated and untreated gDNA by MeDIP using anti-5mC antibody relative to a non-specific IgG demonstrates. Error bars represent the standard error of the mean of three biological replicates. (**D**) Calibration curve, plotting log(chromatin) against Rct for HEC50 treated versus HEC50 untreated. Error bars represent the standard error of the mean of three biological replicates. (**E**) Western blot detection of global acetylated histone 3 (acH3) in HEC50 treated versus HEC50 untreated chromatin using a specific antibody directed against the modified histone protein. (**F**) Enrichment of the human p21 locus associated with acetylated histone H3 by ChIP using 1 µg HEC50 treated untreated chromatin. Error bars represent the standard error of the mean of three biological replicates.

of 'gross' epigenetic status rather than the 'statically global view' obtained from the assimilation of multi-loci epigenome datasets. The speed of signal acquisition compared to PCR or DNA sequencing is substantially improved as there is no requirement for template amplification. Furthermore, the relative simplicity of the analytical process and very low sample volumes lend this approach to clinical utility. This technology is envisioned to become a price competitive point-of-care system, where single use functional screen-printed electrodes are preferable to reusable systems due to the need to minimize false positive results that would likely occur due to incomplete biological sample removal from the biosensor surface. Future miniaturization of this technology, as printing techniques become more refined and with higher resolution, will go some way to reducing the associated waste stream. Current legislation necessitates that clinical samples are correctly handled of therefore sensor chips exposed to clinical material must be disposed of appropriately.

Cytosine methylation and gross histone H3 acetylation are regulatory mechanisms for, and established markers of, transcription repression and activation respectively. DNA methylation directs gene silencing through the establishment of condensed heterochromatic structures, whereas histone H3 acetylation results in the loss of association between lysine residues in histone tails and the negatively charged phosphate backbone of DNA resulting in transition to a euchromatic state. Furthermore, both mechanisms are the target of currently available therapeutics including decitabine, a cytosine analogue that functions as a DNA methylase transferase (DNMT) inhibitor. Following its incorporation into DNA during replication, decitabine irreversible binds to DNMT1, sequestering it the site of interaction and rendering it ineffective. Vorinostat is a histone deacetylase (HDAC) inhibitor that binds to the active site in HDAC enzymes, inhibiting their function, leading to an accumulation of acetylated histones.

Here we have reported differences between EIS measurements as a ΔΩ value, as the exact amount of DNA or chromatin present has not been directly determined. However, as total global DNA methylation levels are estimated to be 0.7–2.8 mol percent i.e., moles of 5-methyl cytosine per 100 bases of total DNA in eukaryotes (Hall, 1971), we estimate for example that 0.52–2.1ng/µL methylated DNA per 75ng/µL input DNA is being detected in the EIS assay. Similarly, it is estimated that only 1.2% of chromatin is acetylated at histone H3 (Roh et al., 2005), therefore we are detecting approximately 1.6 ng/µL acetylated histone H3 per 134ng/µL input chromatin.

DNA methylation levels were similar for non-cancer and cancer breast cell lines tested using EIS suggesting that global methylation without any selection of genetic loci is not useful in differentiating between the cell types used in this study. In contrast, the level of global acetylation in the MCF7 cancer cell line was higher than in the non-cancer MCF12A cells illustrating that, even in the absence of any pharmacological treatment that can modify cellular epigenetic status, differences can be determined between cell types that originate from the same tissue.

Using EIS sensors we were able to trace cellular response to treatments with DNMT or HDAC inhibitors, monitoring the respective decreases in DNA methylation or increases in histone H3 acetylation. The response of both breast and endometrial cancer cells to decitabine and vorinostat was as expected with differentiation between cell responses to either treatment detectable at detectable very low levels of input DNA or chromatin. With this detection platform available it will now be possible to monitor patient responses to treatment directly from patient samples.

With the recent surge in global efforts to map epigenomes across

cancer types and patient cohorts (Bock et al., 2016; Libertini et al., 2016; Rendeiro et al., 2016; Xi et al., 2018) it is becoming possible to associate global epigenetic changes with disease status using statistical approaches. We propose that multiplex EIS could be used to simultaneously assess several epigenetics marks, and that such an approach could accurately diagnose and even stage disease progression directly from patient samples. Such an approach would obviate the need for DNA sequencing or indeed the complex and ongoing processes of identifying and characterizing circulating protein biomarkers. The use of a multi-epigenetic marker algorithm coupled with the $\Delta\Omega$ differential quantification against known and predetermined/preprogrammed standards provides an obvious and compelling strategy that now needs to be exploited.

5. Conclusions

Whilst a number of DNA methylation sensors have been reported (Krejcova et al., 2017) no single platform has yet emerged as a preferred solution for accurate and rapid methylation testing. The use of biosensors in monitoring changes in global methylation levels in response to cancer cell treatment with decitabine is reported here for the first time. The development of biosensors for detection of histone acetylation lags significantly behind that of DNA methylation biosensors, and has to date been limited to fluorescent based approaches (Wang et al., 2017). The system presented in the current study uses an antibody-based approach, and employs the same platform used for DNA methylation detection. Using this system, we were able to demonstrate for the first-time the amplification and label free immuno-detection of histone H3 acetylation, and monitor responses of breast and endometrial cancer models to vorinostat, a drug that has undergone clinical trials for the treatment of advanced breast cancer (Luu et al., 2018). The ability to track patient response to both these drugs will have major implications in the management of their care.

The combined detection of two different epigenetic marks, using a unified detection platform, now opens the way to monitoring multiple epigenetic modifications, particularly targeting the multitude of modifications that occur on histone proteins, which as well as acetylation, include protein methylation, ubiquitylation, phosphorylation, sumoylation, ribosylation and citrullination. Developments in smaller, multiplexed sensors are now required, and could result in a move from SPEs to emerging FET-based systems (Campos et al., 2019).

CRediT authorship contribution statement

S.R. Teixeira: Conceptualization, Resources, Software, Formal analysis. **C.M. Abreu:** Validation, Writing - original draft, Writing - review & editing. **L. Parkes:** Resources, Formal analysis. **J. Davies:** Resources, Formal analysis. **S. Yao:** Resources, Software, Validation. **M.A. Sawhney:** Resources, Software, Validation. **L. Margarit:** Conceptualization, Writing - review & editing. **D. Gonzalez:** Conceptualization, Supervision, Writing - original draft, Writing - review & editing. **I. Mendes Pinto:** Conceptualization, Investigation, Supervision, Validation, Visualization, Writing - original draft, Writing - review & editing. **L.W. Francis:** Conceptualization, Writing - original draft, Writing - review & editing. **R.S. Conlan:** Conceptualization, Funding acquisition, Supervision, Writing - original draft, Writing - review & editing.

Acknowledgments

none

Appendix A. Supplementary data

Supplementary data to this article can be found online at https://doi.org/10.1016/j.bios.2019.111386.

Funding

S.T. Welsh National Research Network in Advanced Engineering and Materials (NRNF77). I.M.P. Marie Curie COFUND Programme "NanoTRAINforGrowth" from the European Union's Seventh Framework Programme for research, technological development and demonstration under grant agreement no 600375. This article is in part a result of the project advancing cancer research: from basic knowledge to application (NORTE-01-0145-FEDER-000029), co-financed by Norte Portugal Regional Operational Programme (NORTE, 2020), under the PORTUGAL 2020 Partnership Agreement, through the European Regional Development Fund.

Competing interests

The authors declare that they have no competing interests.

References

Bock, C., Halbritter, F., Carmona, F.J., Tierling, S., Datlinger, P., Assenov, Y., Berdasco, M., Bergmann, A.K., Booher, K., Busato, F., Campan, M., Dahl, C., Dahmcke, C.M., Diep, D., Fernández, A.F., Gerhauser, C., Haake, A., Heilmann, K., Holcomb, T., Hussmann, D., Ito, M., Kläver, R., Kreutz, M., Kulis, M., Lopez, V., Nair, S.S., Paul, D.S., Plongthongkum, N., Qu, W., Queirós, A.C., Reinicke, F., Sauter, G., Schlomm, T., Statham, A., Stirzaker, C., Strogantsev, R., Urdinguio, R.G., Walter, K., Weichenhan, D., Weisenberger, D.J., Beck, S., Clark, S.J., Esteller, M., Ferguson-Smith, A.C., Fraga, M.F., Guldberg, P., Hansen, L.L., Laird, P.W., Martín-Subero, J.I., Nygren, A.O.H., Peist, R., Plass, C., Shames, D.S., Siebert, R., Sun, X., Tost, J., Walter, J., Zhang, K., 2016. Quantitative comparison of DNA methylation assays for biomarker development and clinical applications. Nat. Biotechnol. https://doi.org/10.1038/nbt.3605.

Bormann, F., Rodríguez-Paredes, M., Lasitschka, F., Edelmann, D., Musch, T., Benner, A., Bergman, Y., Dieter, S.M., Ball, C.R., Glimm, H., Linhart, H.G., Lyko, F., 2018. Cell-of-Origin DNA methylation signatures are maintained during colorectal carcinogenesis. Cell Rep. https://doi.org/10.1016/j.celrep.2018.05.045.

Butler, J.S., Dent, S.Y.R., 2013. The role of chromatin modifiers in normal and malignant hematopoiesis. Blood. https://doi.org/10.1182/blood-2012-10-451237.

Campos, R., Borme, J., Guerreiro, J.R., Machado, G., Cerqueira, M.F., Petrovykh, D.Y., Alpuim, P., 2019. Attomolar label-free detection of dna hybridization with electrolyte-gated graphene field-effect transistors. ACS Sens. 4, 286–293. https://doi.org/10.1021/acssensors.8b00344.

Capp, J.P., 2017. Tissue disruption increases stochastic gene expression thus producing tumors: cancer initiation without driver mutation. Int. J. Cancer. https://doi.org/10.1002/ijc.30596.

Coleman, N., De, S., 2018. Mutation signatures depend on epigenomic contexts. Trends Cancer 4, 659–661.

Daniels, J.S., Pourmand, N., 2007. Label-free impedance biosensors: opportunities and challenges. Electroanalysis. https://doi.org/10.1002/elan.200603855.

Dawson, M.A., Kouzarides, T., 2012. Cancer epigenetics: from mechanism to therapy. Cell 150, 12–27.

Flavahan, W.A., Gaskell, E., Bernstein, B.E., 2017. Epigenetic plasticity and the hallmarks of cancer. Science 80. https://doi.org/10.1126/science.aal2380.

Gazze, A., Ademefun, R., Conlan, R.S., Teixeira, S.R., 2018. Electrochemical impedence spectroscopy enabled CA125 detection; toward early ovarian cancer diagnosis using graphene biosensors. J. Interdiscip. Nanomedicine 3, 82–88. https://doi.org/10.1002/jin2.40.

Graff-Baker, A.N., Orozco, J.I.J., Marzese, D.M., Salomon, M.P., Hoon, D.S.B., Goldfarb, M., 2018. Epigenomic and transcriptomic characterization of secondary breast cancers. Ann. Surg. Oncol. https://doi.org/10.1245/s10434-018-6582-7.

Guo, F., Wang, Y., Liu, J., Mok, S.C., Xue, F., Zhang, W., 2016. CXCL12/CXCR4: a symbiotic bridge linking cancer cells and their stromal neighbors in oncogenic communication networks. Oncogene. https://doi.org/10.1038/onc.2015.139.

Hall, R.H., 1971. The Modified Nucleosides in Nucleic Acids. Columbia University Press 1971.

Jones, P.A., Baylin, S.B., 2007. The epigenomics of cancer. Cell 128, 683–692.

Koo, K.M., Sina, A.A.I., Carrascosa, L.G., Shiddiky, M.J.A., Trau, M., 2015. DNA-bare gold affinity interactions: mechanism and applications in biosensing. Anal. Methods. https://doi.org/10.1039/c5ay01479d.

Krejcova, L., Richtera, L., Hynek, D., Labuda, J., Adam, V., 2017. Current trends in electrochemical sensing and biosensing of DNA methylation. Biosens. Bioelectron. 97, 384–399. https://doi.org/10.1016/J.BIOS.2017.06.004.

Libertini, E., Heath, S.C., Hamoudi, R.A., Gut, M., Ziller, M.J., Czyz, A., Ruotti, V., Stunnenberg, H.G., Frontini, M., Ouwehand, W.H., Meissner, A., Gut, I.G., Beck, S., 2016. Information recovery from low coverage whole-genome bisulfite sequencing. Nat. Commun. https://doi.org/10.1007/s00227-009-1360-5.

Lo, P.K., Zhou, Q., 2018. Emerging techniques in single-cell epigenomics and their applications to cancer research. J. Clin. Genomics 1, 1–8.

Luu, T., Kim, K. pyo, Blanchard, S., Anyang, B., Hurria, A., Yang, L., Beumer, J.H., Somlo, G., Yen, Y., 2018. Phase IB trial of ixabepilone and vorinostat in metastatic breast cancer. Breast Canc. Res. Treat. 167, 469–478. https://doi.org/10.1007/s10549-017-4516-x.

Mossman, D., Kim, K.T., Scott, R.J., 2010. Demethylation by 5-aza-2'-deoxycytidine in colorectal cancer cells targets genomic DNA whilst promoter CpG island methylation persists. BMC Canc. https://doi.org/10.1186/1471-2407-10-366.

Qu, K., Zaba, L.C., Satpathy, A.T., Giresi, P.G., Li, R., Jin, Y., Armstrong, R., Jin, C., Schmitt, N., Rahbar, Z., Ueno, H., Greenleaf, W.J., Kim, Y.H., Chang, H.Y., 2017. Chromatin accessibility landscape of cutaneous T cell lymphoma and dynamic response to HDAC inhibitors. Cancer Cell. https://doi.org/10.1016/j.ccell.2017.05.008.

Ramos, M.P., Wijetunga, N.A., McLellan, A.S., Suzuki, M., Greally, J.M., 2015. DNA demethylation by 5-aza-2′-deoxycytidine is imprinted, targeted to euchromatin, and has limited transcriptional consequences. Epigenet. Chromatin. https://doi.org/10.1186/s13072-015-0004-x.

Rendeiro, A.F., Schmidl, C., Strefford, J.C., Walewska, R., Davis, Z., Farlik, M., Oscier, D., Bock, C., 2016. Chromatin accessibility maps of chronic lymphocytic leukaemia identify subtype-specific epigenome signatures and transcription regulatory networks. Nat. Commun. https://doi.org/10.1038/ncomms11938.

Roh, T.Y., Cuddapah, S., Zhao, K., 2005. Active chromatin domains are defined by acetylation islands revealed by genome-wide mapping. Genes Dev. https://doi.org/10.1101/gad.1272505.

Sánchez, S., Roldán, M., Pérez, S., Fàbregas, E., 2008. Toward a fast, easy, and versatile immobilization of biomolecules into carbon nanotube/polysulfone-based biosensors for the detection of hCG hormone. Anal. Chem. https://doi.org/10.1021/ac7025282.

Sawhney, M., Conlan, R., 2019. POISED-5, a portable on-board electrochemical impedance spectroscopy biomarker analysis device. Biomed. Microdevices. https://doi.org/10.1007/s10544-019-0406-9.

Sheahan, A.V., Ellis, L., 2018. Epigenetic reprogramming: a key mechanism driving therapeutic resistance. Urol. Oncol. 36, 375–379.

Singh, A.A., Petraglia, F., Nebbioso, A., Yi, G., Conte, M., Valente, S., Mandoli, A., Scisciola, L., Lindeboom, R., Kerstens, H., Janssen-Megens, E.M., Pourfarzad, F., Habibi, E., Berentsen, K., Kim, B., Logie, C., Heath, S., Wierenga, A.T.J., Clarke, L., Flicek, P., Jansen, J.H., Kuijpers, T., Yaspo, M.L., Della Valle, V., Bernard, O., Gut, I., Vellenga, E., Stunnenberg, H.G., Mai, A., Altucci, L., Martens, J.H.A., 2018. Multi-omics profiling reveals a distinctive epigenome signature for high-risk acute promyelocytic leukemia. Oncotarget. https://doi.org/10.18632/oncotarget.25429.

Stewart, C.M., Tsui, D.W.Y., 2018. Circulating cell-free DNA for non-invasive cancer management. Cancer Genet. https://doi.org/10.1016/j.cancergen.2018.02.005.

Teixeira, S., Conlan, R.S., Guy, O.J., Sales, M.G.F., 2014a. Label-free human chorionic gonadotropin detection at picogram levels using oriented antibodies bound to graphene screen-printed electrodes. J. Mater. Chem. B 2, 1852–1865. https://doi.org/10.1039/c3tb21235a.

Teixeira, S., Conlan, R.S., Guy, O.J., Sales, M.G.F., 2014b. Label-free human chorionic gonadotropin detection at picogram levels using oriented antibodies bound to graphene screen-printed electrodes. J. Mater. Chem. B 2, 1852. https://doi.org/10.1039/c3tb21235a.

Teixeira, S.R., Lloyd, C., Yao, S., Andrea Salvatore, Gazze, Whitaker, I.S., Francis, L., Conlan, R.S., Azzopardi, E., 2016. Polyaniline-graphene based α-amylase biosensor with a linear dynamic range in excess of 6 orders of magnitude. Biosens. Bioelectron. https://doi.org/10.1016/j.bios.2016.05.034.

Wang, H., Li, Y., Zhao, K., Chen, S., Wang, Q., Lin, B., Nie, Z., Yao, S., 2017. G-quadruplex-based fluorometric biosensor for label-free and homogenous detection of protein acetylation-related enzymes activities. Biosens. Bioelectron. 91, 400–407. https://doi.org/10.1016/j.bios.2016.12.065.

Xi, Y., Shi, J., Li, Wenqian, Tanaka, K., Allton, K.L., Richardson, D., Li, J., Franco, H.L., Nagari, A., Malladi, V.S., Coletta, L. Della, Simper, M.S., Keyomarsi, K., Shen, J., Bedford, M.T., Shi, X., Barton, M.C., Lee Kraus, W., Li, Wei, Dent, S.Y.R., 2018. Histone modification profiling in breast cancer cell lines highlights commonalities and differences among subtypes. BMC Genomics. https://doi.org/10.1186/s12864-018-4533-0.

Zhang, J., Han, X., Gao, C., Xing, Y., Qi, Z., Liu, R., Wang, Y., Zhang, X., Yang, Y.G., Li, X., Sun, B., Tian, X., 2018. 5-Hydroxymethylome in circulating cell-free DNA as A potential biomarker for non-small-cell lung cancer. Genom. Proteom. Bioinform. https://doi.org/10.1016/j.gpb.2018.06.002.

Zhu, C., Yang, G., Li, H., Du, D., Lin, Y., 2015. Electrochemical sensors and biosensors based on nanomaterials and nanostructures. Anal. Chem. https://doi.org/10.1021/ac5039863.

Zor, E., Hatay Patir, I., Bingol, H., Ersoz, M., 2013. An electrochemical biosensor based on human serum albumin/graphene oxide/3-aminopropyltriethoxysilane modified ITO electrode for the enantioselective discrimination of d- and l-tryptophan. Biosens. Bioelectron. https://doi.org/10.1016/j.bios.2012.10.068.